universe

MDPI

Conference Report

Ions, Protons, and Photons as Signatures of Monopoles

Vicente Vento

Departamento de Física Teórica-IFIC, Universidad de Valencia-CSIC, 46100 Burjassot (Valencia), Spain; vicente.vento@uv.es

Received: 8 October 2018; Accepted: 1 November 2018; Published: 7 November 2018

Abstract: Magnetic monopoles have been a subject of interest since Dirac established the relationship between the existence of monopoles and charge quantization. The Dirac quantization condition bestows the monopole with a huge magnetic charge. The aim of this study was to determine whether this huge magnetic charge allows monopoles to be detected by the scattering of charged ions and protons on matter where they might be bound. We also analyze if this charge favors monopolium (monopole–antimonopole) annihilation into many photons over two photon decays.

1. Introduction

The theoretical justification for the existence of classical magnetic poles, hereafter called monopoles, is that they add symmetry to Maxwell's equations and explain charge quantization. Dirac showed that the mere existence of a monopole in the universe could offer an explanation of the discrete nature of the electric charge. His analysis leads to the Dirac Quantization Condition (DQC) [1,2]

$$eg = N/2, \ N = 1, 2, ..., \tag{1}$$

where e is the electron charge, g the monopole magnetic charge, and we use natural units $\hbar = c = 1 = 4\pi\varepsilon_0$. Monopoles have been a subject of experimental interest since Dirac first proposed them in 1931.

In Dirac's formulation, monopoles are assumed to exist as point-like particles and quantum mechanical consistency conditions lead to establish the value of their magnetic charge. Because of of the large magnetic charge as a consequence of Equation (1), monopoles can bind in matter [3]. In the case of the Dirac monopole theory, the other monopole parameter is its mass. Searches for direct monopole production have been performed in most accelerators. The lack of monopole detection has been transformed into monopole mass lower bounds [4–7]. Experiments at the Large Hadron Collider (LHC) have probed higher masses [8–13]. Hereafter, we shall assume that the monopole mass is larger than 400 GeV.

This study contains three contributions. The first deals with the detection of monopoles in matter. For that purpose, we study the scattering of charged particles by monopoles bound in matter and eliminate the matter background using Rutherford backscattering techniques. The presentation is based on Reference [14]. The second contribution deals with direct scattering of beam particles with monopoles. This contribution is indicated for high-energy collider experiments given the large expected mass of the monopole. We assume that a pair monopole–antimonopole (or a highly-excited monopolium state) is produced and these two particles due to their huge magnetic charge create a very strong magnetic moment which acts on the beam particles producing a characteristic scattering scenario. The third contribution deals with the disintegration of the monopole–antimonopole pairs (monopolium) into photons. In the past, most studies have been associated with the disintegration into two photons in analogy with positronium. However, lately, several authors have realized that the huge magnetic charge might favor disintegration into many photons. We present this discussion in Section 4 based on the work of Reference [15]. We end this paper with some conclusions.

2. Ion Scattering off Bound Monopoles

Since monopoles are stable after formation, they may bind into conventional materials like beam pipes, other detector elements, the beam dump or magnetic monopole trapping volumes as in the MoEDAL experiment [10–13]. The aim here was to study the collision of charged ions with bound monopoles to obtain signatures for monopole detection. However, since the monopole will be surrounded in practice by a huge (Avogadro's number) of conventional nuclei, to isolate the monopole signal from conventional ion-nucleus Rutherford scattering, we propose the use of backscattering techniques.

2.1. Scattering of a Charged Spin 1/2 *Particle Using a Spinless Magnetic Monopole*

Let us assume the following scenario, a beam of charged particles is scattered on a monopole bound in matter. For the time being, we omit the scattering of the particles on the background and study the problem of the scattering of a relativistic particle by the central potential of a monopole field. In a beautiful paper, Kazama, Yang, and Goldhaber described the scattering of a relativistic spin 1/2 particle with charge Ze by a fixed spinless magnetic monopole [16]. The formulation developed in terms of fiber bundles, which is lacking the string singularity, obtains the result by the use of monopole harmonics [17]. The result for the differential cross section for an unpolarized beam is given by

$$\frac{d\sigma}{d\Omega} = \frac{1}{2k^2}\left(|T_{|q|}|^2 + 2q^2(\sin(\theta/2))^{4|q|-2}\right), \tag{2}$$

where $q = Zeg = Z/2$, θ is the scattering angle and the function $T_{|q|}$ is a complex expression defined by Equation (80) of Reference [16]. Its behavior is similar for low q to the conventional Rutherford formula as can be seen in Figure 1 where we plot

$$Ratio(q,\theta) = \left(\frac{Z'e}{gv}\right)^2 \left(\frac{d\sigma}{d\Omega} \Big/ \frac{d\sigma}{d\Omega_R}\right) \tag{3}$$

for a beam of particles of velocity v, charge Ze scattered by a target particle of charge $Z'e$ for f $q = 0.5, 2, 4, 6$. This ratio is independent of beam momentum. The ratio varies dramatically with Z, especially in the backward direction where the cross section is smallest.

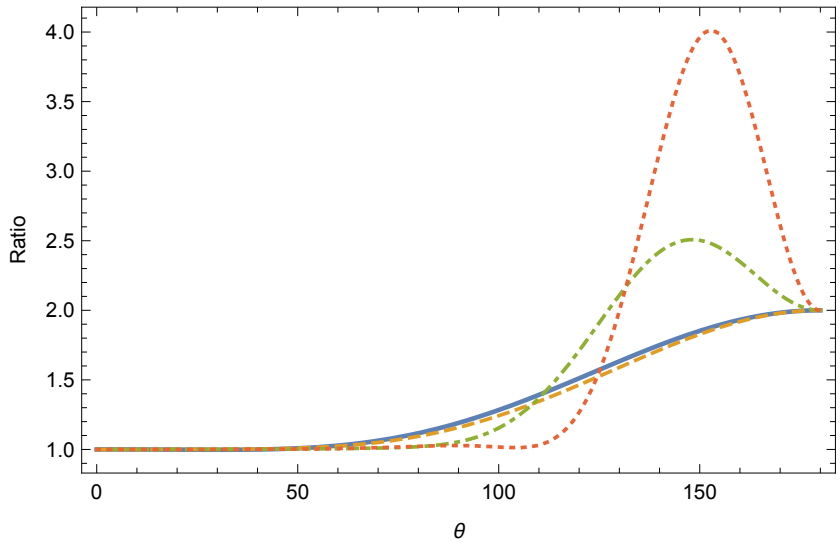

Figure 1. Plot of the functions $R(q,\theta)$ defined in Equation (3) for $q = 1/2$ (solid), $q = 2$ (dashed), $q = 4$ (dotdashed), and $q = 6$ (dotted).

In Figure 2, we plot the differential cross section for a beam of 1 GeV/nucleon ions of $^{41}_{20}$Ca. We note that the presence of a monopole close to the beam makes the probability of scattered ions coming out transverse and backward to the beam measurable.

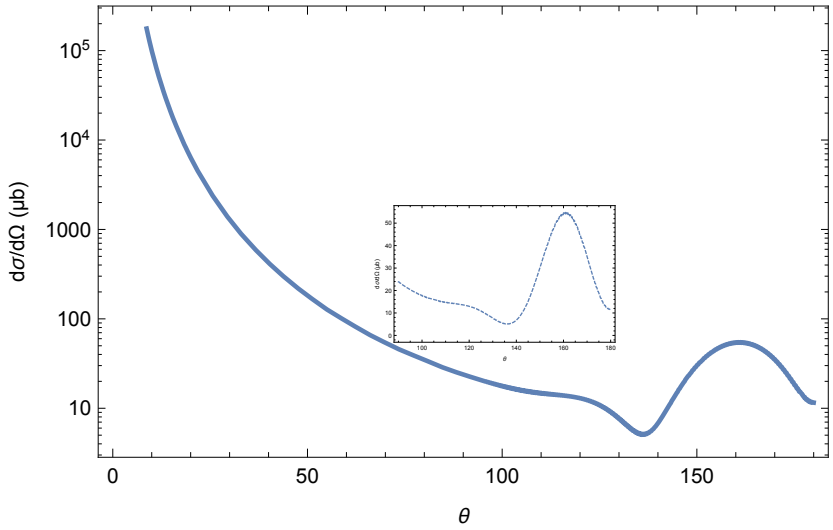

Figure 2. Elastic scattering ion monopole cross section (μ b) a for a beam energy of 1 GeV/nucleon spin 1/2 ions ($^{41}_{20}$Ca) by a fixed spinless magnetic monopole. The inset shows in dashed the details of the backward region of experimental interest.

Moving from this approximation of infinitely massive monopoles to monopoles with a finite mass does not change the result much [14] because the expected masses of the monopole are supposed to be greater than 400 GeV [4–7,12].

We might conclude this discussion by stating that a monopole sends beam particles of known momentum (elastic scattering) into the transverse and backward directions which are easy to detect. We also notice that the structure in the backward direction as shown in Figure 1 can be very different from the traditional Rutherford scattering. Those two features are clear signals of the existence of bound monopoles.

2.2. Backscattering Spectrography

The ion-monopole cross section is large, however, since the probes are macroscopic, the monopoles will be surrounded by a huge number, $\sim 10^{24}$, of conventional scatterers and therefore the background might hide the monopole signal.

To avoid this problem we recall the Rutherford backscattering technique of condensed matter physics [18]. We consider the elastic scattering of a particle in the beam with mass m_b and a stationary particle of mass m_t located in the sample. Let us consider the kinematics of a non-relativistic collision with $m_b >> k$ we recall that the energy of the scattered projectile E_f is reduced from the initial energy E_i by the so called kinematical factor $E_f = \kappa E_i$, where

$$\kappa = \frac{m_b \cos\theta_L \pm \sqrt{m_t^2 - m_b^2(\sin\theta_L)^2}}{m_b + m_t}, \tag{4}$$

where θ_L is the scattering angle of the projectile in the laboratory frame. The plus sign is taken when the mass of the projectile is less than that of the target, otherwise the minus sign is taken. Equation (4) is a consequence of energy momentum conservation. This equation shows that if $m_b > m_t$ for certain angles, the square root admits no real solution and therefore there is an angular sector were scattering is strictly forbidden by energy momentum conservation. We plot the κ factor in Figure 3.

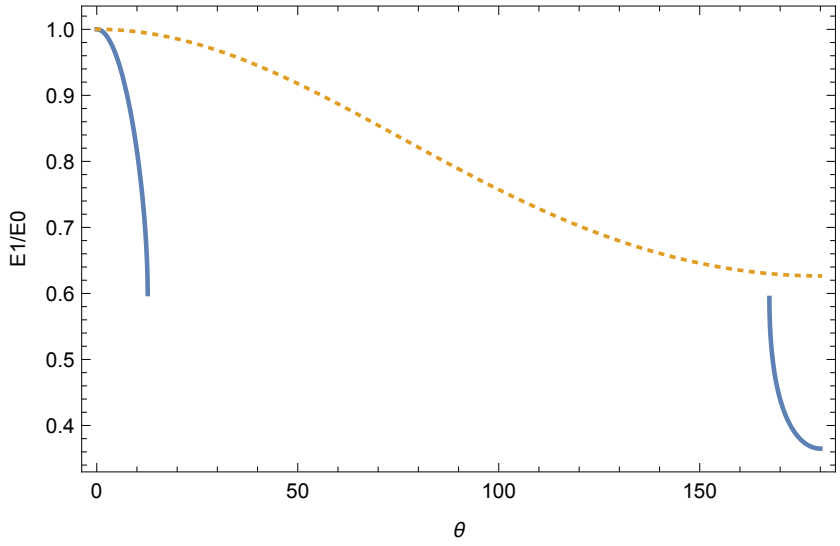

Figure 3. Kinematical factor for $^{41}_{20}$Ca on $^{9}_{4}$Be at beam energy of 1 GeV/nucleon(solid), and for $^{41}_{20}$Ca on a monopole whose mass is taken to be $10m_{41}$.

The generalization to relativistic kinematics of Equation (4) is straightforward but less transparent for visualizing the kinematical restriction [19]. Thus, scanning the probe with a beam of particles whose atomic number is greater than any atomic number in the probe there will be no background in a large angular region and therefore we will obtain a clean signal if monopoles are bound in the probe.

Given the lack of a fundamental theory with well known parameters for monopole production, it is very unlikely that our technique might substitute the much cheaper use of magnetometers. However, one can use monopole detection via ion scattering as a parasitic experiment with little additional equipment. For example, a monopole bound to the beam pipe of an accelerator, can be detected by the set up used for Central Exclusive Production (CEP) [19,20] by carrying out a van der Meer sweeping with the ion beam, or if bound in the material of the beam dump, it can be detected by locating a few detectors for beam particles backward of the beam impact region.

3. Ion and Proton Scattering on Monopole–Antimonopole Pairs

The Large Hadron Collider is reaching energies never achieved before allowing the search for exotic particles in the TeV mass range. In a continuing effort to find monopoles, we discuss new signatures to detect them. Hereafter, we study the effect of the magnetic dipole field created by a monopole–antimonopole pair on the successive bunches of charged particles. The scenario, a monopole–antimonopole pair produced close to threshold generates a strong magnetic dipole whose field influences the particles of the beam leading to a well-known scattering pattern. The appearance of these patterns not only provided us with discovery, but given the proposed mechanism, with a narrow mass range which allowed confirmation by other means.

Scattering of Charged Particles by a Magnetic Dipole

Suppose that at the LHC a monopole–antimonopole pair is produced by any of the studied mechanisms [3,21] close to threshold so that it moves very slowly away from the interaction region. The pair produces a magnetic dipole field in the beam line which affects the successive non-interacting particles in the bunches. We reduce this scenario at this point to the theoretical problem of the scattering of a beam of charged particles by a fixed magnetic dipole potential.

The scattering cross section of charged particles by a dipole potential in the Born approximation can be easily calculated in the non-relativistic case [22],

$$\frac{d\sigma}{d\omega}(\theta)|_{nr} = \frac{4m_b^2 q^2}{k^4}\left(\frac{\sin\left(kdsin\theta\right)}{1-\cos\theta}\right)^2 \tag{5}$$

where $q = Zeg$, k is the beam momentum, m_b the mass of the particles in the beam with charge Ze, and the magnetic charges are located at $z = +d$ and $z = -d$. By assuming that the scattered wave is much smaller than the incoming wave, we estimate the validity of the Born approximation which is given by

$$\left|\frac{m_b q\pi}{k}\right| << 1. \tag{6}$$

Since for LHC $k >> m_b q$ this condition is satisfied. For example, for a Pb ion beam at 2.760 TeV per nucleon the factor is 0.0466 and for a proton beam at 7 TeV is 0.0002.

This non-relativistic treatment can be generalized to a relativistic treatment with some restrictions which do not apply here leading to [23]

$$\frac{d\sigma}{d\omega}(\theta) = \frac{E^2 - k^2\sin\left(\theta/2\right)}{m_b^2}\frac{d\sigma}{d\omega}(\theta)|_{nr}. \tag{7}$$

We plot the results of some calculations in Figure 4 to analyze the behavior of the cross section. We display the cross section for protons at 7 TeV LHC energies and a separation between the poles of 0.01 fm to show the oscillating structure of the cross section. The magnitude of the distance has been simply chosen for graphic reasons. We expect the actual distance to be much larger and not stable but slowly increasing. We also draw as a dotted line the envelop of maxima of the cross section. The right plot in Figure 4 shows how the oscillations frequency changes as we double the distance between the poles. The bigger the distance the higher the oscillation frequency. However, and this is very important for experimental arguments, the envelope of the maxima does not change since it is determined by the charges and the kinematics and not by the distance between the poles. In the real process, the poles will slowly be separating and therefore the oscillating frequency will be increasing and thus the actual experimental cross section will very much resemble the dotted representation of the envelope of maxima.The total cross section stabilizes as can be seen in Figure 5. These results show that a signature of monopole–antimonopole creation is the emission of highly energetic charged beam particles in the transverse direction with a specific distribution. It is important to note that in this case, the full beam scatters on the dipole potential and therefore the full luminosity of the LHC beam will contribute to the scattering. However, we do not expect the dipole to be active for very long since monopole and anti-monopole will fly apart or disintegrate into photons.

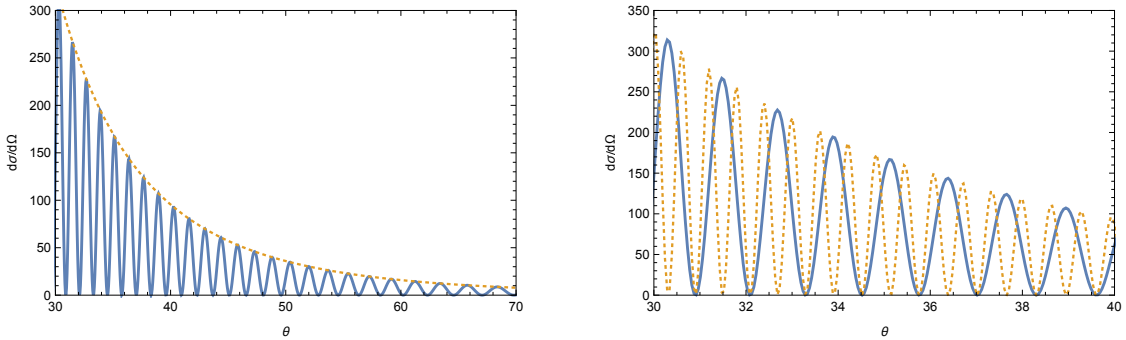

Figure 4. The figure on the left shows the elastic scattering of proton beam of 7 TeV (solid) by a dipole, with a distance between the poles of 0.01 fm. The dotted line represents the envelope of the maxima. The figure on the left shows the effect as we double the pole distance: the shape and position of the oscillations change but the maximum magnitude remains the same.

The experiment can also be carried out with ion beams. Two factors make up the difference: a momentum-mass effect which leads to a factor $\frac{Z^2}{A^2}$, Z being the number of protons and A the atomic number which reduces the cross section; the beam momentum, which for ions is much lower than 2.76 TeV, and leads to a larger cross section (see Equation (5)). Both effects tend to compensate for the LHC running conditions and thus the cross section for both proton and ion experiments would be very similar.

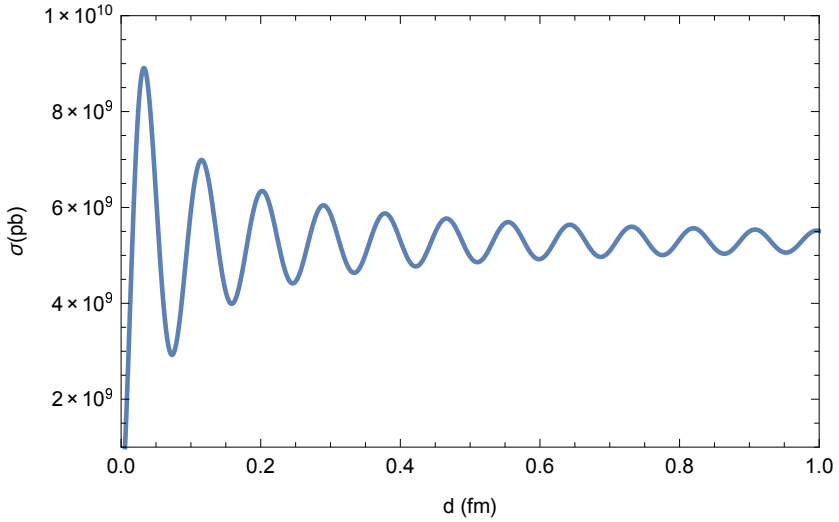

Figure 5. We show the magnitude of the total scattering cross section for a proton at 7 TeV in picobarn as a function of interpole distance parameter d in fm.

The signature of the presence of monopoles in the interaction region is a Rutherford type cross section with many highly energetic beam particles coming out in the transverse direction. The signature of these particles could be used as a trigger for monopole detection.

Inspired by an old idea originating from Dirac and Zeldovich [1,2,24], we proposed that monopolium, a bound state of monopole anti-monopole [24,25] could be easier to detect experimentally than free monopoles [26,27]. Monopolium could be formed in high-energy collisions at the LHC [26,27]. If monopolium is produced in a highly excited state it will possess an electric dipole moment and our calculation also produces a similar signature for monopolium. The suitability of the experiments just described depends on the magnitude of the background produced by the elastic scattering of beam particles and the length of the lifetime of the monopole–antimonopole states.

4. Monopole–Antimonopole Disintegration into Many Photons

The annihilation of monopolium into two photons has been a matter of intense study [21,28]. It has been recently shown that monopolium might annihilate most preferably into many low-energy photons [15,28,29]. This result motivates experimental investigation of monopolium and monopole–antimonopole by looking into multi-photon decay [15].

The two and four photon decay channels of the ground state parapositronium have been studied in QED. In particular, the two photon channel is known up to $O(\alpha^3 \log^2 \alpha)$ [30–33] and the four photon decay has been studied up to order $O(\alpha)$ [34], where α is the fine structure constant. We show for the ratio of these channels the result to Leading Order [35,36],

$$\frac{\Gamma_4}{\Gamma_2} = 0.277 \left(\frac{\alpha}{\pi}\right)^2. \tag{8}$$

The factor in front of the coupling constant, 0.277, contains the contribution of the 4! diagrams of the four photon amplitude and the 2! diagrams of the two photon one, to the lowest order. The binding

energy is very small, a few eV, and has been neglected in the calculation, therefore the energy factors cancel in the ratio.

Let us assume that the monopole-photon coupling is analogous to the electron-photon coupling except for an effective vertex characterized by the dressed monopole magnetic charge g [37]. Thus, we extend the positronium calculation to monopolium just by changing $e \to g$. Recalling the parapositronium calculation in terms of the coupling we get,

$$\frac{\Gamma_4}{\Gamma_2} \sim F_{42}\left(\frac{\alpha_g}{\pi}\right)^2 \quad \cdots \quad \frac{\Gamma_{2n}}{\Gamma_2} \sim F_{2n2}\left(\frac{\alpha_g}{\pi}\right)^{2n-2}, \tag{9}$$

where $\alpha_g = \frac{1}{4\alpha} \sim \frac{137}{4} \sim 34.25$ obtained from Dirac's Quantization Condition (DQC) [1,2]. The F's represent the contribution of all the Feynman amplitudes to the process shown as subindex after extracting the contribution of the magnetic charge, which is explicitly shown. For example, to the leading order, $F_{42} \approx 0.277$ as seen in Equation (8). We perform the calculations, as is customarily done in monopole physics, to the leading order. As a result of the large magnetic coupling, the calculations can give a qualitative indication of magnitudes at most, which is what we can pursue at present. At the end of our analysis we comment on how non-perturbative effects might affect our calculation.

In Figure 6, we show one of the $2n!$ contributions to the amplitude for a $2n$ photon decay to leading order, and we note that these types of contributions in the above ratios are determined only by vertices and propagators. The calculation for high n with $2n!$ diagrams is out of the scope of any study. Let us first discuss an educated estimation for large n. In the rest frame of the bound system, the annihilation into many photons leads to an average momentum for each photon much smaller than the mass of monopolium and therefore much smaller than the mass of the monopole. In order to make an estimation of the above ratios, we consider that in the propagators, the monopole mass dominates over the momentum and therefore the calculation of the width, in units of monopole mass, depends exclusively on three factors: the number of diagrams $(2n)!$, the photons' symmetry factor $1/(2n)!$, and the phase space of the outgoing massless particles, namely

$$(phsp)^{2n} = \frac{1}{2}\frac{1}{(4\pi)^{4n-3}}\frac{M^{4n-4}}{\Gamma(2n)\Gamma(2n-1)}, \tag{10}$$

where M is the monopolium mass and $n = 1, 2, 3, \ldots$ being $2n$ the number of photons emitted.

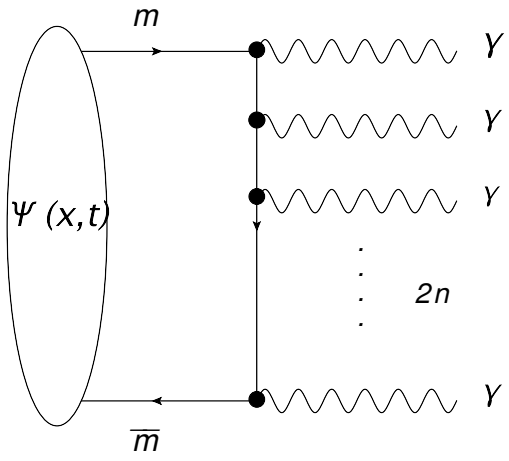

Figure 6. One of the $2n!$ multi-photon emission diagrams.

With all these approximations we obtain the expression

$$\frac{\Gamma_{2n}}{\Gamma_2} = \left(\frac{\alpha_g}{\pi}\right)^{2n-2}\left(\frac{M}{2m}\right)^{4n-4}\frac{2n!}{2!(2n-1)!(2n-2)!}. \tag{11}$$

Note that this equation leads to $\Gamma_2/\Gamma_2 = 1$ and for $n = 2$ and $M = 2m$, one recovers the parapositronium case, $\Gamma_4/\Gamma_2 = \left(\frac{\alpha_g}{\pi}\right)^2$, with the interference factor missing (recall Equation (8)). In order to incorporate this effect, we make a second estimate. In the first estimate, we have assumed p^2 to be very small compared with m^2 in the propagator an approximation valid for large n. Let us assume for the second estimate that on the contrary $p^2 \sim m^2$, an approximation which might be adequate for small n. This approximation introduces into Equation (11) a factor $(\frac{1}{2})^{2n-2}$ leading to

$$\frac{\Gamma_{2n}}{\Gamma_2} = \left(\frac{1}{2}\right)^{2n-2} \left(\frac{\alpha_g}{\pi}\right)^{2n-2} \left(\frac{M}{2m}\right)^{4n-4} \frac{2n!}{2!(2n-1)!(2n-2)!}. \tag{12}$$

For $n = 2$, this factor is 0.25, which is very close to true calculation to leading the order 0.277. This factor is extremely suppressing for large n, where the approximations discussed initially might be better. We show results with and without this factor to determine a region of confidence. If the leading order calculation were all there was, the true result would be between these two limiting expressions. We discuss possible non-perturbative effects at the end of the analysis. In our expressions, we consider the effect of the binding energy not taken into account in the conventional positronium analysis.

In Figure 7, we plot Equations (11) and (12) for two different binding energies and we get bell-shape distributions. For small binding energies ($M \approx 2m$), the value of n on the average is $\overline{n} \sim 7$ with a deviation of $\Delta n \sim \pm 2$. For large binding energies ($M \sim m$), the average value of n is $\overline{n} \sim 3$ with a deviation of $\Delta n \sim \pm 1$. If the interference factor is included, the multiplicity ($2\overline{n}$) is reduced to $\overline{n} \sim 4$ with $\Delta n \sim \pm 1$ for small binding and $\overline{n} \sim 2$ with $\Delta n \sim \pm 1$ for large binding. Thus, the multiplicity decreases as the binding energy increases. However, even with the strongly suppressing interference factor included, four photon emission is favored.

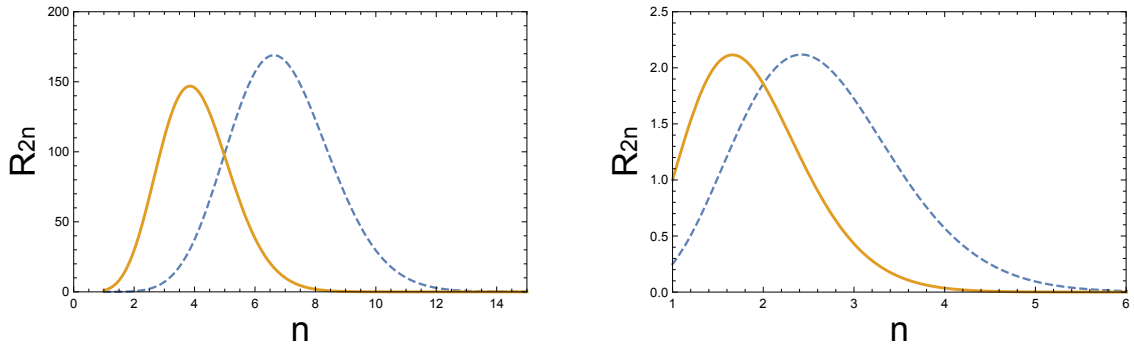

Figure 7. The Γ_{2n}/Γ_2 ratio as a function of n calculated according to Equations (11) and (12). The left figure is for zero binding energy and the right figure for $E_b \sim m$. The solid curves represent the calculation with the interference factor and the dashed curves the one without the factor. In order to have the two curves at the same scale, the no interference ratios had to be divided by 250 left and by 4 right.

We next study the dependence of multiplicity with the binding energy. To do so, we find the maximum of the ratio in Equations (11) and (12) as a function of binding energy. The result is plotted in Figure 8, where we show the binding energy in units of monopole mass as a function of the average photon multiplicity in the annihilation. The outcome is clear, large average multiplicities, 8–12 photons, arise if the binding energy is small, $M \sim 2m$, while smaller average multiplicities, 4–6 photons, occur for large bindings, $M \sim m$. In the latter case, considerable rates extend up to multiplicities of 8 photons as is shown in Figure 7, right.

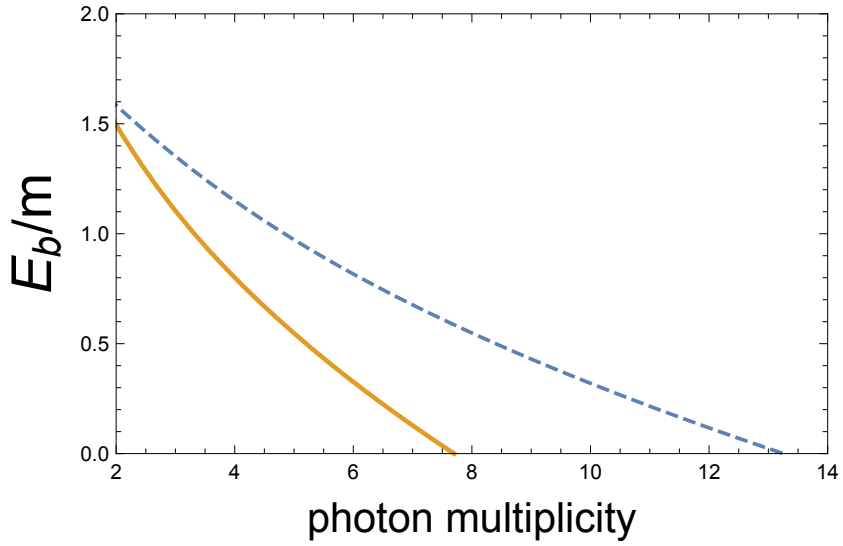

Figure 8. Binding energy in units of monopole mass as a function of average photon multiplicity in the annihilation. The solid curve represents the calculation with interference factor while the dashed curve is that without that factor.

We can get an analytic formula for the most probable photon decay channel by calculating the maximum of the logarithm of Equations (11) and (12) using Sterling's formula ($k! \sim k^k e^{-k}\sqrt{2\pi k}$). Sterling's formula is quite good even for low k, i.e., for $k = 2$ it gives 1.919, for $k = 3$ it gives 5.836, and $k = 4$ it gives 23.506. Thus, we can consider the equations we are going to derive good approximations for any n. Let us write a generic interference factor $(\delta)^{n-1}$ in front of Equation (11) which for $\delta = 1$ gives Equation (11) itself and for $\delta = 0.25$ Equation (12). The values of n for the maximum decay rates are given by the solutions of the equation

$$n = \frac{\alpha_g\sqrt{\delta}}{2\pi}\left(1 - \frac{E_b}{2m}\right)^2 \exp(\frac{1}{4n}) + 1, \tag{13}$$

for specific values of δ and the binding energy E_b. For large n, which occurs for small binding energy, we get the approximate solution

$$n \approx \frac{\alpha_g\sqrt{\delta}}{2\pi} + 1, \tag{14}$$

which is very illuminating because it shows explicitly the effect of the coupling constant in increasing the photon multiplicities as seen numerically in Figure 7.

All the approximations used thus far are valid for Dirac's original formulation. The so called β-coupling scheme leads to small effective couplings close to threshold [3,21,28]. We have analyzed its consequences in Reference [15], which we can summarize by saying that close to threshold the two photon decay is the dominant process, but given that β rises rapidly [21,28], the present analysis holds slightly away from threshold.

Finally, we would like to make some comments about non-perturbative effects. Given the large value of the coupling constant, it is evident that our calculation is merely qualitative and aimed at proposing new signals to discover monopoles at lower photon energies. Let us assume for the following discussion the worst possible scenario, namely that non-perturbative effects make the multi-photon channels weaker. We parametrize the non-perturbative effects by an effective δ. How small can δ get to make four and six photon decay ratios irrelevant? We use Equation (13) for $n = 2, 3$ and plot δ as a function of binding energy in Figure 9.

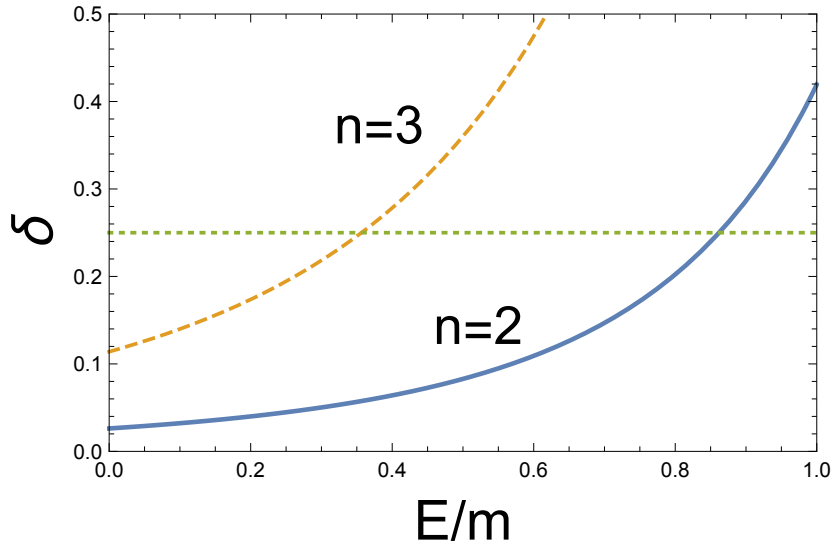

Figure 9. The interference factor δ as a function of binding energy for four and six photon decays according to Equation (13).

From the figure it is apparent that a small bound monopolium produces preferably multi-photon decays up to very small interference factors. As the binding energy increases, the possibility of multi-photon decays decreases. Note, however, that the four photon decay is greater or comparable to two photon decays up to interference factors many times smaller than the one used in this calculation and note that monopole–antimonopole annihilation behaves much like zero binding monopolium.

5. Conclusions

The discovery of monopoles would be a major breakthrough in our understanding of charge quantization and would imply revisiting Quantum Electrodynamics in a strong coupling regime. Monopoles are stable particles and they bind to conventional matter, specifically to the nuclei of atomic systems [3]. Several techniques have been used to detect monopoles [38], in particular, the most common is to measure the magnetic charge of matter probes with magnetometers [11–13]. The large coupling constant and mass of the monopoles single out this particle with respect to the abundant conventional particles that might surround them. An intelligent use of ion beams in parasitic experiments might lead to the detection of monopoles by eliminating the conventional background by borrowing a technique that condensed matter physicists use to detect impurities [18]. Beam particles, protons or ions, can scatter from monopole–antimonopole pairs or monopolium produced in colliders leading to a well defined scattering pattern which can be detected by small implementations in ongoing experiments. Finally, we have shown that a large multiplicity of photon events might also be a signal for the discovery of monopoles.

Funding: This research was funded by Mineco and UE Feder under contract FPA2016-77177-C2-1-P and SEV-2014-0398.

Acknowledgments: I would like to thank Fernando Martínez, Philippe Mermod and Risto Orava for discussions regarding ion and proton monopole scattering. I would like to thank Huner Fanchiotti and Carlos A. García Canal who collaborated with me in the study of monopolium (monopole–antimonopole) multiphoton annihilation. I also acknowledge the hospitality extended to me by the IFLP/CONICET and Departamento de Física de la Universidad Nacional de La Plata were some of this research was carried out. I am grateful to Nick Mavromatos and Vassia Mitsou for the invitation to present my work in this conference.

Conflicts of Interest: The author declare no conflict of interest.

References

1. Dirac, P.A.M. Quantised singularities in the electromagnetic field. *Proc. R. Soc. Lond. A* **1931**, *133*, 60–72. [CrossRef]

2. Dirac, P.A.M. The Theory of magnetic poles. *Phys. Rev.* **1948**, *74*, 817. [CrossRef]
3. Milton, K.A. Theoretical and experimental status of magnetic monopoles. *Rep. Prog. Phys.* **2006**, *69*, 1637. [CrossRef]
4. Abulencia, A.; Acosta, D.; Adelman, J.; Affolder, T.; Akimoto, T.; Albrow, M.G.; Ambrose, D.; Amerio, S.; Amidei, D.; Anastassov, A.; et al. Direct search for Dirac magnetic monopoles in $p\bar{p}$ collisions at $\sqrt{s} = 1.96$ TeV. *Phys. Rev. Lett.* **2006**, *96*, 201801. [CrossRef] [PubMed]
5. Fairbairn, M.; Kraan, A.C.; Milstead, D.A.; Sjostrand, T.; Skands, P.Z.; Sloan, T. Stable massive particles at colliders. *Phys. Rep.* **2007**, *438*, 1–63. [CrossRef]
6. Bbiendi, G.; Ainsley, C.; Åkesson, P.F.; Alexander, G.; Anagnostou, G.; Anderson, K.J.; Asai, S.; Axen, D.; Bailey, I.; Barberio, E.; et al. Search for Dirac magnetic monopoles in e+e- collisions with the OPAL detector at LEP2. *Phys. Lett. B* **2008**, *663*, 37–42. [CrossRef]
7. ATLAS Collaboration. Search for magnetic monopoles in $\sqrt{s} = 7$ TeV pp collisions with the ATLAS detector. *Phys. Rev. Lett.* **2012**, *109*, 261803. [CrossRef] [PubMed]
8. ATLAS Collaboration. Search for magnetic monopoles and stable particles with high electric charges in 8 TeV pp collisions with the ATLAS detector. *Phys. Rev. D* **2016**, *93*, 052009. [CrossRef]
9. Lenz, T. Searches for long-lived and highly-ionizing particles at the CMS and ATLAS experiments. *PoS LHCP* **2016**, *2016*, 104–113.
10. Acharya, B.; Alexandre, J.; Bernabéu, J.; Campbell, M.; Cecchini, S.; Chwastowski, J.; De Montigny, D.; Derendarz, A.; De Roeck, J.R.; Ellis, M.; et al. The Physics Programme of the MoEDAL Experiment at the LHC. *Int. J. Mod. Phys. A* **2014**, *29*, 1430050. [CrossRef]
11. Acharya, B.; Alexandre, J.; Bendtz, K.; Benes, P.; Bernabéu, J.; Campbell, M.; Cecchini, S.; Chwastowski, J.; Chatterjee, A.; de Montigny, M.; et al. Search for magnetic monopoles with the MoEDAL prototype trapping detector in 8 TeV proton-proton collisions at the LHC. *J. High Energy Phys.* **2016**, *2016*, 67. [CrossRef]
12. Acharya, B.; Alexandre, J.; Baines, S.; Benes, P.; Bergmann, B.; Bernabéu, J.; Branzas, H.; Campbell, M.; Caramete, L.; Cecchini, S.; et al. Search for Magnetic Monopoles with the MoEDAL Forward Trapping Detector in 13 TeV Proton-Proton Collisions at the LHC. *Phys. Rev. Lett.* **2017**, *118*, 061801. [CrossRef] [PubMed]
13. Acharya, B.; Alexandre, J.; Baines, S.; Benes, P.; Bergmann, B.; Bernabéu, J.; Branzas, H.; Campbell, M.; Caramete, L.; Cecchini, S.; et al. Search for magnetic monopoles with the MoEDAL forward trapping detector in 2.11 fb^{-1} of 13 TeV proton-proton collisions at the LHC. *Phys. Lett. B* **2018**, *782*, 510–516. [CrossRef]
14. Vento, V. Ion scattering on monopoles. *arXiv* **2018**, arXiv:1809.04504.
15. Fanchiotti, H.; Garcia Canal, C.A.; Vento, V. Multiphoton annihilation of monopolium. *Int. J. Mod. Phys. A* **2017**, *32*, 1750202. [CrossRef]
16. Kazama, Y.; Yang, C.N.; Goldhaber, A.S. Scattering of a Dirac Particle with Charge Ze by a Fixed Magnetic Monopole. *Phys. Rev. D* **1977**, *15*, 2287. [CrossRef]
17. Wu, T.T.; Yang, C.N. Dirac Monopole Without Strings: Monopole Harmonics. *Nucl. Phys. B* **1976**, *107*, 365–380. [CrossRef]
18. Feldman, L.C.; Mayer, J.W. *Fundamentals of Surface and Thin Film Analysis*; North-Holland: New York, NY, USA, 1986.
19. Orava, R.; Vento, V. Can we use the proton beam at LHC to detect monopoles? Unpublished work, 2018.
20. McNulty, R. Central Exclusive Production at LHCb. *arXiv* **2017**, arXiv:1711.06668.
21. Epele, L.N.; Fanchiotti, H.; Canal, C.A.G.; Mitsou, V.A.; Vento, V. Looking for magnetic monopoles at LHC with diphoton events. *Eur. Phys. J. Plus* **2012**, *127*, 60. [CrossRef]
22. Weinberg, S. *Lectures in Quantum Mechanics*; Cambridge University Press: Cambridge, UK, 2015.
23. Parzen, G. On the Scattering Theory of the Dirac Equation. *Phys. Rev.* **1950**, *80*, 261. [CrossRef]
24. Zeldovich, Y.B.; Khlopov, M.Y. On The Concentration Of Relic Magnetic Monopoles in the Universe. *Phys. Lett. B* **1978**, *79*, 239–241. [CrossRef]
25. Hill, C.T. Monopolonium. *Nucl. Phys. B* **1983**, *224*, 469–490. [CrossRef]
26. Vento, V. Hidden Dirac Monopoles. *Int. J. Mod. Phys. A* **2008**, *23*, 4023–4037. [CrossRef]
27. Epele, L.N.; Fanchiotti, H.; Garcia Canal, C.A.; Vento, V. Monopolium: The Key to monopoles. *Eur. Phys. J. C* **2008**, *56*, 87–95. [CrossRef]
28. Epele, L.N.; Fanchiotti, H.; Garcia Canal, C.A.; Vento, V. Can the 750 GeV enhancement be a signal of light magnetic monopoles? *arXiv* **2016**, arXiv:1607.05592.

29. Barrie, N.D.; Sugamoto, A.; Yamashita, K. Construction of a model of monopolium and its search via multiphoton channels at LHC. *Prog. Theor. Exp. Phys.* **2016**, *2016*, 113B02. [CrossRef]
30. Penin, A.A. High order QED corrections in physics of positronium. *Int. J. Mod. Phys. A* **2004**, *19*, 3897–3904. [CrossRef]
31. Lepage, G.P.; Mackenzie, P.B.; Streng, K.H.; Zerwas, P.M. Multi-Photon Decays of Positronium. *Phys. Rev. A* **1983**, *28*, 3090. [CrossRef]
32. Khriplovich, I.B.; Yelkhovsky, A.S. On the radiative corrections $\alpha^2 \ln \alpha$ to the positronium decay rate. *Phys. Lett. B* **1990**, *246*, 520–522. [CrossRef]
33. Czarnecki, A.; Karshenboim, S.G. Decays of positronium. *arXiv* **1999**, arXiv:hep-ph/9911410.
34. Adkins, G.S.; Pfahl, E.D. Order-a radiative correction to the rate for parapositronium decay to four photons. *Phys. ReV. D* **1998**, *59*, R915. [CrossRef]
35. Billoire, A.; Lacaze, R.; Morel, A.; Navelet, H. The OZI Rule Violating Radiative Decays of the Heavy Pseudoscalars. *Phys. Lett.* **1978**, *78*, 140–143. [CrossRef]
36. Muta, T.; Niuya, T. Nonplanar Four Jets in Quarkonium Decays as a Probe for Three Gluon Coupling. *Prog. Theor. Phys.* **1982**, *68*, 1735–1748. [CrossRef]
37. Zwanziger, D. Local Lagrangian quantum field theory of electric and magnetic charges. *Phys. Rev. D* **1971**, *3*, 880. [CrossRef]
38. Patrizii, L.; Spurio, M. Status of Searches for Magnetic Monopoles. *Annu. Rev. Nucl. Part. Sci.* **2015**, *65*, 279–302. [CrossRef]